ELSEVIER

International Journal of Heat and Fluid Flow 22 (2001) 188–200

International Journal of HEAT AND FLUID FLOW

www.elsevier.com/locate/ijhff

Time- and space-resolved heat transfer characteristics of single droplet cooling using microscale heater arrays

Jungho Lee, Jungho Kim *, Kenneth T. Kiger

Department of Mechanical Engineering, 2181 Glenn L. Martin Hall, University of Maryland, College Park, MD 20742-3035, USA

Received 18 August 2000; accepted 23 October 2000

Abstract

Heat transfer by phase change has long been an attractive method of cooling since large amounts of heat can be removed with relatively small temperature differences. The current study focuses on making detailed measurements of the heat flux and interfacial motion of an isolated droplet as it impacts an isothermal surface at low and moderate superheats. The heat flux measurements were made using a novel 96-element, feedback-controlled heater array, which allowed the local, instantaneous heat flux to be resolved. The dynamics of the droplet were visualized using a synchronized high-speed digital camera. The experiments were performed at three superheats ($T_w - T_{sat} = 9°C$, 19°C and 29°C), with nominally constant droplet diameter (0.82 mm) and impact velocity (0.3 m/s). The accuracy of the measurement was checked by calculating the energy required to vaporize a droplet of a known mass, and show agreement to within 4%. The results show that the vaporization process can be divided into two parts; a first part which is characterized by a transient effective heat transfer coefficient, and a second part in which the heat transfer coefficient is constant. The details provided by the measurements show that the initial transient in h is not simply due to an unsteady conduction process, but is also affected by the drop deformation dynamics and external diffusive vapor region near the impact site. The second part of the evaporation process is compared to models proposed in the literature for droplets which maintain a constant contact angle, and is found to be in good agreement.

Keywords: Single droplet cooling; Droplet heat transfer; Microscale heater

1. Introduction

The use of liquid droplets to cool heated surfaces is an important process in several industrial applications due to the large amounts of energy that can be extracted from the wetted surface at relatively low temperatures through the latent heat of evaporation. For example, spray cooling might be used to remove large amounts of energy from electronic devices while keeping temperature gradients small and junction temperatures below 85°C. Through tailoring the spray pattern, spray cooling can be used to obtain high heat transfer rates coupled with good temperature uniformity across the sprayed surface, which is important in microelectronics where even small temperature gradients across the chip can cause component failure. Unfortunately, the work to date has largely been empirical, and a lack of predictive capability regarding spray cooling exists due to the complex nature of the heat removal process. With this motivation, the goal of the current work is to examine the fundamental behavior of the transient heat transfer characteristics of a dynamically impacting droplet, which represents a first step towards understanding the more complex problem of a complete spray.

When a droplet strikes a heated surface, it flattens into a thin disk or splat whose thickness is much smaller than the diameter of the droplet, and high heat fluxes can be obtained due to the formation and evaporation of a thin liquid film on the heated surface. The controlling physical mechanism of the vaporization process depends on the degree of superheat applied to the heated surface. There are three distinct superheat regimes in connection with droplet vaporization from hot surfaces (Sadhal et al., 1997) – these are commonly referred to as the low, intermediate, and high superheat regime. In the low superheat case, the liquid droplet maintains contact with the surface, and nucleate boiling is typically suppressed for sufficiently thin drops. At intermediate superheat, nucleation takes place and heat transfer is enhanced. With increasing surface temperature, however, the droplet does not maintain continuous contact with the surface and the heat transfer rate decreases. In the high superheat regime, a stable vapor layer is formed between the droplet and the heated surface. In this regime, the droplet does not contact the solid wall and the heat transfer is limited mainly by conduction through a vapor layer. This mechanism is commonly referred to as the Leidenfrost phenomena.

* Corresponding author. Tel.: +301-405-5437; fax: +301-314-9477.
E-mail address: kimjh@eng.umd.edu (J. Kim).

0142-727X/01/$ - see front matter
PII: S0142-727X(00)00082-5

Notation

A	area of microscale heater array (m^2)
A_{av}	time averaged area of splat (m^2)
A_D	area of splat (m^2)
c_p	specific heat (J/kg K)
D	splat diameter (m)
D_0	initial splat diameter (m)
d_{eq}	equivalent droplet diameter (m)
d_0	initial droplet diameter (m)
h	heat transfer coefficient (W/m^2 °C)
h_{av}	average heat transfer coefficient (W/m^2 °C)
h_{cal}	calculated heat transfer coefficient (W/m^2 °C)
h_v	heat transfer coefficient due to vapor (W/m^2 °C)
h_{fg}	heat of vaporization (J/kg)
k	thermal conductivity (W/m^2 °C)
m_d	mass of droplet (kg)
Q_e	energy required to evaporate a droplet (J)
Q_{meas}	measured total energy required to evaporate a droplet (J)
q	heat rate (W)
q''	heat flux (W/cm^2)
q''_{liq}	heat flux into the liquid (W/cm^2)
q''_{nc}	natural convection heat flux (W/cm^2)
q''_{raw}	total heat flux (W/cm^2)
q''_{sc}	substrate conduction heat flux (W/cm^2)
R_l	thermal resistance of liquid (°C/W)
R_{th}	thermal resistance (°C/W)
R_v	thermal resistance of vapor (°C/W)
T_a	ambient temperature (°C)
T_0	initial droplet temperature (°C)
T_{sat}	saturation temperature (°C)
T_w	local wall temperature (°C)
t_{e1}	first stage evaporation time (s)
t_{e2}	second stage evaporation time (s)
t_e	total evaporation time ($= t_{e1} + t_{e2}$) (s)
t^*	dimensionless evaporation time ($= t/t_e$)
V	volume of droplet (m^3)
V_0	initial volume of droplet (m^3)
V_i	voltage across the individual ith heater element
v	impact velocity of droplet (m/s)

Greeks

α	thermal diffusivity ($= k/\rho c_p$)
β	spread ratio ($= D/d_0$)
δ	average film thickness (m)
δ_{min}	minimum film thickness to support nucleation (m)
ε	effectiveness of evaporation
μ	kinematic viscosity (kg/m s)
θ	liquid–solid contact angle (°)
θ_0	initial contact angle
θ_r	receding contact angle
ρ_d	liquid density (kg/m^3)
ρ_v	vapor density (kg/m^3)
σ	surface tension (kg/s^2)

Numerous investigations of the theoretical and experimental evolution of single droplet cooling heat transfer have been presented in literature reviews by Bolle and Moureau (1982) and Sadhal et al. (1997). Wachters and Westerling (1966) and Wachters et al. (1966) examined the kinematic motion of a single droplet impacting a hot surface using high-speed photographs above the Leidenfrost temperature. McGinnis and Holman (1969) investigated the effect of droplet velocity and impact frequency on the heat transfer rate, but also at temperatures above Leidenfrost. Toda (1972, 1974) reported extensive measurements of an evaporating water droplet and proposed a heat transfer model based on three regions (low temperature, transitional, and high temperature), according to the thermal behavior of the thin liquid film formed on the heated surface. Bonacina et al. (1979) performed experiments at low enough water flow rates to avoid the formation of a thin liquid film on the heated surface, resulting in a droplet evaporative cooling process. Liu and Yao (1982) introduced a model of spray cooling heat transfer based on the different heat transfer mechanisms involved in each region, and interpreted the contribution of each mechanism to the overall heat transfer. This model was again used by Choi and Yao (1987) in a study of spray cooling in the nucleate and film boiling regimes. Di Marzo and Evans (1989) performed a significant amount of work for droplet evaporation on surfaces below the saturation temperature.

The present study was motivated by the need for an effective method of removing the high heat fluxes generated in compact electronic devices. Most such devices must operate at temperatures lower than 85°C, so the saturation temperature of the coolant should be well below this temperature. PF-5060 is such a dielectric coolant, having a saturation temperature of 56°C at atmospheric pressure. The properties of PF-5060 are identical to those of FC-72 (3M Corporation, 1995). The properties of PF-5060 are compared with those of water at Table 1.

Table 1
Physical properties of PF-5060 at 25°C and 1 atm

Property	Fluids	
	PF-5060	Water
Chemical formula	C_6F_{14}	H_2O
Boiling point (°C)	56	100
Density (ρ) (kg/m^3)	1680	997
Dynamic viscosity (μ) (kg/m s)	0.672×10^{-3}	0.901×10^{-3}
Kinematic viscosity (v) (m^2/s)	0.4×10^{-6}	0.904×10^{-6}
Surface tension (σ) (kg/s^2)	0.012	0.072
Specific heat (c_p) (J/kg K)	1046.5	4180
Thermal conductivity (k) (W/m K)	0.057	0.611
Latent heat (h_{fg}) (kJ/kg)	87.9	2442.3

In the present study, the time- and space-resolved heat transfer characteristics for a single droplet impacting a heated surface were experimentally measured, and the results are compared to a model of droplet evaporation. The local wall heat flux and temperature measurements were made using a novel experimental technique in which 96 individually controlled heaters were used to map the heat transfer coefficient contour on the surface. The droplet behavior was also simultaneously viewed using a high-speed digital video camera.

2. Single droplet cooling model

A two stage model of droplet evaporation was proposed by Di Marzo and Evans (1989); De Marzo et al. (1993), and Qiao and Chandra (1997). A schematic of single droplet behavior and a typical side view of the droplet are shown in Fig. 1. In the first stage, the contact splat diameter D remains constant

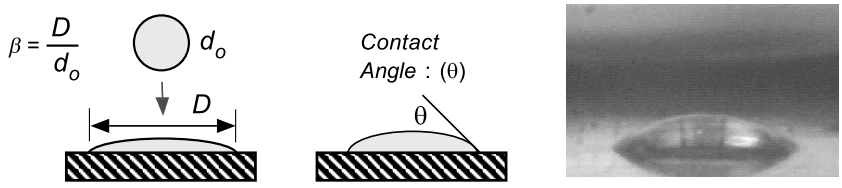

Fig. 1. Schematic of single droplet and typical side view of droplet at 65°C.

while the contact angle θ decreases from its initial value θ_0 to a receding value θ_r. In the second stage, the contact angle θ remains constant at θ_r while the splat diameter decreases.

The heat transfer coefficient for the droplet is defined as

$$h = \frac{q''_{liq}}{T_w - T_a}. \tag{1}$$

An energy balance on the droplet is given by

$$hA(T_w - T_a) = -\rho_d h_{fg} \frac{dV}{dt}, \tag{2}$$

where V is the volume of the droplet. V can be approximated by assuming the droplet is a segment of a sphere (Sadhal and Plesset, 1979):

$$V = \frac{\pi D^3}{24} \frac{(1-\cos\theta)^2(2+\cos\theta)}{\sin^3\theta}. \tag{3}$$

If h is assumed to be constant, then integrating Eq. (2) yields the value of h to be

$$h = \frac{V_0 \rho_d h_{fg}}{A_{av}(T_w - T_a)t_e}, \tag{4}$$

where A_{av} is the time averaged contact area

$$A_{av} = \frac{1}{t_e}\int_0^{t_e} \frac{\pi}{4} d_0^2 \beta^2(t)\, dt \tag{5}$$

and t_e is the evaporation time for the droplet.

2.1. First stage of evaporation

During the first stage when the droplet diameter is the initial splat diameter D_0, the time rate of change of the droplet volume is given by

$$\frac{dV}{dt} = \frac{\pi D_0^3}{8}\left[\frac{1}{(1+\cos\theta)^2}\right]\frac{d\theta}{dt}. \tag{6}$$

Substituting Eq. (6) into Eq. (2) and integrating between θ_0 and θ_r assuming h to be constant yields the time required for the first stage:

$$t_{e1} = \frac{\rho_d h_{fg} D_0}{4h(T_w - T_a)}\left[\tan\left(\frac{\theta_0}{2}\right) - \tan\left(\frac{\theta_r}{2}\right) + \frac{1}{3}\left(\tan^3\left(\frac{\theta_0}{2}\right) - \tan^3\left(\frac{\theta_r}{2}\right)\right)\right]. \tag{7}$$

2.2. Second stage of evaporation

During the second stage when the contact angle is equal to the receding contact angle ($\theta = \theta_r$) the time rate of change of the droplet volume is expressed by

$$\frac{dV}{dt} = \frac{\pi D^2}{8}\left[\frac{(1-\cos\theta_r)^2(2+\cos\theta_r)}{\sin^3\theta_r}\right]\frac{dD}{dt}. \tag{8}$$

Substituting Eq. (8) into Eq. (2) and again assuming h is constant yields the rate at which the splat diameter changes with time:

$$\frac{dD}{dt} = -2h(T_w - T_a) \Big/ \rho_d h_{fg}\left[\frac{(1-\cos\theta_r)^2(2+\cos\theta_r)}{\sin^3\theta_r}\right]. \tag{9}$$

Note that the splat diameter varies linearly for the given assumptions. Integrating yields the evaporation time t_{e2} required for the second stage:

$$t_{e2} = \frac{\rho_d h_{fg} D_0}{2h(T_w - T_a)}\left[\frac{(1-\cos\theta_r)^2(2+\cos\theta_r)}{\sin^3\theta_r}\right]. \tag{10}$$

This paper uses this model to determine the relative magnitude of the heat transfer resistance within the liquid to that of the vapor during droplet evaporation. Validation of the model described above is performed, and conclusions regarding the evaporation mechanism are made.

3. Experimental apparatus

An array of 96 individually controlled heaters was used to measure the heat flux distribution on the surface as a function of time and space. Feedback loops similar to those used in constant temperature anemometry are used to vary the voltage across each heater in the array to keep its temperature (resistance) constant, essentially eliminating the possibility of heater burnout. The electronics and heater array allowed for heat fluxes of up to 160 W/cm^2. The focus of the current experiments was to study the transient heat transfer distribution on the surface for given droplet impact parameters at three different superheats (85°C, 75°C, and 65°C).

3.1. Microscale heater array

Local surface heat flux and temperature measurements were provided by a serpentine platinum resistance heater element, similar to what was used in previous publications (Rule et al., 1998; Rule and Kim, 1999; Rule et al., 1999). Each heater was 270×270 μm^2 in size. The platinum heater lines were 5 μm wide, about 400 nm thick, spaced 5 μm apart, and about 600 μm in total length. Each heater had an electrical resistance of about 750 Ω. The 96 individual heaters were arranged in a square array about 2.7 mm on a side. A photograph of the microscale heater array is shown in Fig. 2. The aluminum lines that supply power to the heaters were routed between the heaters to the edge of the array. Up to 17 heater arrays were fabricated simultaneously on a single quartz wafer using VLSI circuit fabrication techniques. Platinum was sputtered onto the entire wafer, the heaters were masked off, and the platinum was removed from the unmasked areas using an ion milling process. Aluminum was then vapor-deposited onto the surface, the aluminum power leads were masked off, and the remaining aluminum was removed using a wet chemical etch. As a final step, a layer of SiO_2 was deposited

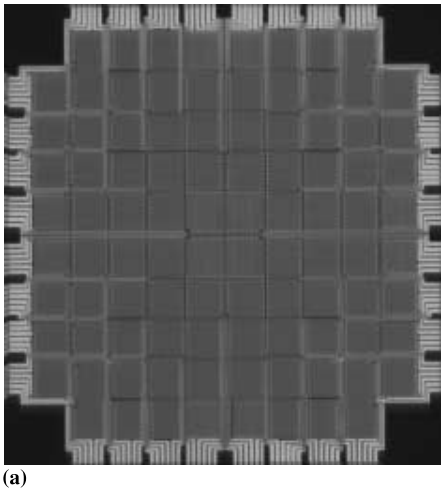

(a)

	96	95	94	93	92	91	90	89	
65	37	64	63	62	61	60	59	58	88
66	38	17	36	35	34	33	32	57	87
67	39	18	5	16	15	14	31	56	86
68	40	19	6	1	4	13	30	55	85
69	41	20	7	2	3	12	29	54	84
70	42	21	8	9	10	11	28	53	83
71	43	22	23	24	25	26	27	52	82
72	44	45	46	47	48	49	50	51	81
	73	74	75	76	77	78	79	80	

(b)

Fig. 2. Arrangement of 96 microscale heater arrays, with non-functional heaters represented by black squares: (a) photo of 96 microscale heater array; (b) arrangement of 96 microscale heater array, with non-functional heaters represented by black squares.

over the heater array to provide the surface with a uniform surface energy. The completed quartz wafer was diced into chips, each containing a single heater array. The chips were mounted on a pin-grid-array (PGA) package using epoxy adhesive, and the pins of the PGA were connected to the power leads of the heater array chip using a conventional wire-bonding technique. The completed package was then mounted in a PGA socket that was connected to the control and data-acquisition apparatus.

3.2. Feedback control circuit

The temperature of heat heater in the array was kept at *constant temperature* by feedback circuits similar to those used in constant temperature anemometry (Fig. 3). The electronics used in this series of tests were similar to those used in previous tests, and are described in detail in Bae et al. (1999). The op-amp measured the imbalance in the bridge and output whatever voltage was needed to bring the bridge into balance. The heater resistance, and thus the heater temperature, was controlled by varying the resistance of a digital potentiometer from Dallas Semiconductor (DS1267). This chip consists of two 10 kΩ digital potentiometers, each having 256 wiper positions. The two potentiometers in this chip were connected in series to make a single 20 kΩ potentiometer with 512 wiper positions. Control of the wiper position was performed through a 3-wire serial interface to a personal computer and digital I/O card. For the resistor values indicated, a heater of nominally 750 Ω resistance could be varied over a 260 Ω range. The heaters have a temperature coefficient of resistance of nominally $0.002°C^{-1}$, providing a temperature range of approximately 175°C. Since the digital potentiometer had 512 settings, the temperature of the heaters could be changed in 0.34°C increments. The large 200 KΩ resistor at the top of the bridge was used to provide a small trickle current through the heater, and resulted in a voltage across the heater of about 100 mV even when the op-amp was not regulating. The output of the circuit (V_{out}) was the voltage required to keep the heater at a set temperature. The heat dissipated by a given heater can be directly obtained from this voltage and the heater resistance.

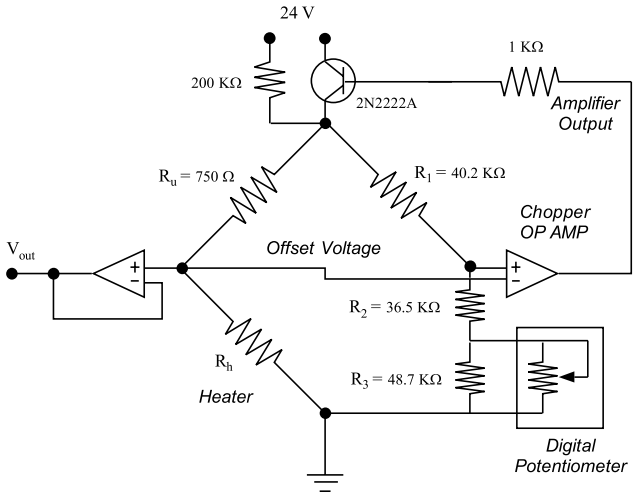

Fig. 3. Schematic of electronic feedback loop.

Sixteen of these circuits were constructed on a single card. Six of these cards plug into a motherboard that routed the signals from the host computer to the individual feedback circuits. The reader is referred to Bae et al. (1999) for additional details regarding the circuit.

3.3. Heater calibration

The heater array was calibrated in an insulated, circulating constant temperature oil bath that was held within 0.2°C of the calibration temperature. Calibration consisted of finding the digital potentiometer wiper position that caused the feedback loop to just begin regulating for a given bath temperature. The uncertainty in threshold wiper position was 1 position, or about 0.34°C in heater temperature.

3.4. Test conditions, set up and data acquisition systems

A schematic of the test apparatus is shown in Fig. 4. The drops were produced by allowing fluid to drip from a glass nozzle onto the heater array. The working fluid used in this study was PF-5060, which effectively replaces CFC-113 as a dielectric coolant. No effort was made to degas the liquid prior to use.

Three sets of experiments were conducted with the heater array set at temperatures of 85°C, 75°C, and 65°C. The release height of the droplets was kept constant, and all of the droplets

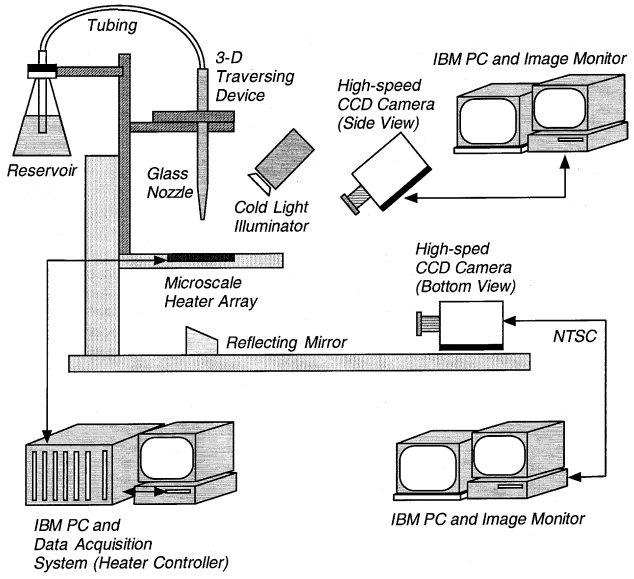

Fig. 4. Schematic of experimental apparatus.

pinched off from the glass nozzle with a nominal diameter of 0.82 mm and impacted the heater array with a nominal velocity of 0.3 m/s. A summary of the droplet initial conditions is shown in Table 2.

The semi-transparent nature of the heater array enabled images to be made of the droplets evaporating on the surface from below using a High-Speed CCD camera (Vision Research Phantom 500 V 3.0) set at 500 fps and 512×512 resolution with a 3.5X tele/microscope lens (Infinity Model KC lens with IF4 objective). Pictures were also taken from the side using another high-speed digital video camera (Kodak Motion Corder Analyzer SR Ultra), set at 512×480 resolution and 250 fps and a second microscope lens (Infinity model K2, with STD objective). Recording was initiated using the same trigger signal sent to the data acquisition system, allowing heat transfer measurements to be synchronized with the high-speed images. The side-view images were used to calculate the initial diameter of the droplet, the impact velocity, and the contact angle during the evaporation process. The impact velocity was calculated by measuring the droplet displacement between successive frames from the high-speed images. The diameter of the splat was measured from both the side-view and the bottom-view of the heater array. Based upon the resolution and depth-of-focus of the images, the uncertainty in the initial drop size and impact velocity is approximately 5%.

The data acquisition system consisted of two A/D boards (Computer Boards CIO-DAS6402-12) installed in a PC, and was capable of sampling the output of each heater at speeds up to 3.3 kHz with 12 bits of resolution. This system was used to obtain time-resolved data at 3000 samples/s from each heater for 5.0 s. Data acquisition was triggered by the rising edge of a TTL signal from the computer and data was stored to disk.

4. Data reduction and uncertainty analysis

The instantaneous power required to keep each heater at a constant temperature was measured and used to determine the heat flux from each heater element. Because all the heaters in the array were at essentially the same temperature, heat conduction between adjacent heaters was negligible. The total heat flux measured for each heater (q''_{raw}), however, needed to be corrected to account for substrate conduction. q''_{raw} could be lost through the bottom by conduction through the substrate (q''_{sc}), through the top by natural convection to the air before droplet impacts (q''_{nc}), or into the liquid after droplet impact (q''_{liq}). In all of the cases studied, q''_{nc} was much smaller than either q''_{sc} or q''_{liq} and could be neglected. Before the droplet impacted the heater array, the power supplied to each heater was lost only by substrate conduction. Because the heaters were held at constant temperature, the substrate conduction remained constant even after droplet impact, enabling the heat transferred from the heaters to the liquid to be determined by subtracting q''_{sc} from q''_{raw}.

The uncertainty in the final heat flux values resulted from uncertainties in q''_{raw}, q''_{nc}, and q''_{sc}. Uncertainties in q''_{raw} were relatively small since they were computed directly from the measured voltage across the heaters and since the heater resistances did not change much. The maximum uncertainty in the voltage across the heater was 0.02 V. The uncertainty in heater resistance was about 1 Ω. Since the heater resistance was nominally 750 Ω, the % uncertainty in heater resistance was about 0.14%.

The uncertainty of the local heat flux measurements was estimated for a typical heater voltage of 2 V using the method suggested by Kline and McClintock (1953). The estimated uncertainty in q''_{raw} was about 2%. The uncertainties in q''_{nc} and q''_{sc} were estimated to be about 5% and 2%, respectively. The uncertainty in q''_{nc} could be large, but it contributed very little to the final uncertainty, since the actual value of q''_{nc} was very small compared to q''_{sc} (q''_{nc} was about 5% of that of q''_{sc}). The final uncertainty in the heat flux was therefore small compared to the uncertainty in droplet diameters (4%). The uncertainty in droplet diameter translated into a much larger uncertainty when computing the energy required to evaporate it because of the dependence on d_0^3.

5. Results and discussion

5.1. Droplet flow visualization

Time resolved evolution of the droplet deformation viewed from beneath the heater array with the heaters set at 65°C are shown in Fig. 5. The droplet reaches its maximum diameter at approximately $t = 4$ ms, after which the droplet recoils and reaches a minimum diameter at $t = 10$ ms. The cycle repeats

Table 2
Experimental parameters in this study

Heater temperature (°C)	Droplet diameter (mm)	Droplet velocity (m/s)	Weber number	Reynolds number
85	0.82	0.31	10.8	629
75	0.83	0.32	11.6	657
65	0.82	0.31	11.1	635

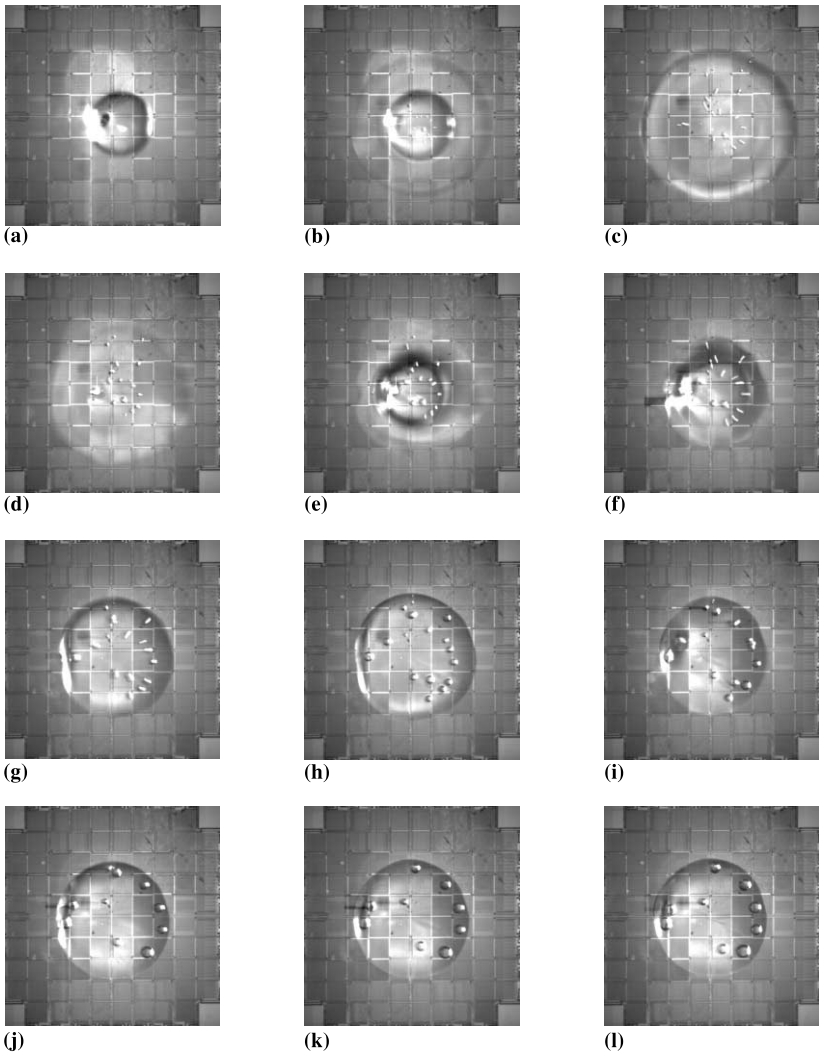

Fig. 5. Evolution of droplet at heater temperature of 65°C: (a) $t = 0$ ms; (b) $t = 2$ ms; (c) $t = 4$ ms; (d) $t = 6$ ms; (e) $t = 8$ ms; (f) $t = 10$ ms; (g) $t = 12$ ms; (h) $t = 14$ ms; (i) $t = 18$ ms; (j) $t = 22$ ms; (k) $t = 26$ ms; (l) $t = 30$ ms.

several times until the motion is sufficiently damped by viscosity around 30 ms.

Snapshots of the drop at three superheats 100 ms after impact is shown on Fig. 6. At the highest superheat (85°C), boiling within the drop is though to occur. At the two lower superheats, bubbles within the drops were seen, but it is thought that these are due to dissolved gas coming out of solution. These observations are supported by additional evidence from the transient heat flux measurements to be discussed below.

5.2. Contact angle and wetting parameter

The time-resolved variation in the liquid–solid contact angle θ is shown in Fig. 7(a). The uncertainty in the measurement of contact angles is $\pm 5°$, while the uncertainty in contact diameter is ± 0.03 mm. The contact angle is seen to change with temperature. Large contact angles for the 85°C case were expected since boiling within the droplet caused its volume to increase. The contact angles for the 75°C case might be larger than those for the 65°C case due to more gas coming out of solution.

The spreading ratio ($\beta = D/d_0$) obtained from the side view, high-speed images are shown in Fig. 7(b). It is seen that β varies similarly for all three superheats if the time is normalized by the evaporation time. The curves are characterized by an initial sharp spike followed by approximately two more spikes as the droplet spreads and recoils before viscosity damps out the oscillatory motion.

5.3. Energy balance

The energy transferred from the wall to the drop can be obtained by integrating the measured wall heat transfer over all the heaters and the entire droplet evaporation time:

$$Q_{\text{meas}} = \sum_{t=0}^{t=t_e} \sum_{i=1}^{N} q_i''(t) A_i \Delta t. \tag{11}$$

This energy can be converted into an equivalent droplet diameter (d_{eq}) using an energy balance on the drop

$$Q_e = \rho_d \pi \frac{d_{\text{eq}}^3}{6} [c_p (T_{\text{sat}} - T_0) + h_{fg}]. \tag{12}$$

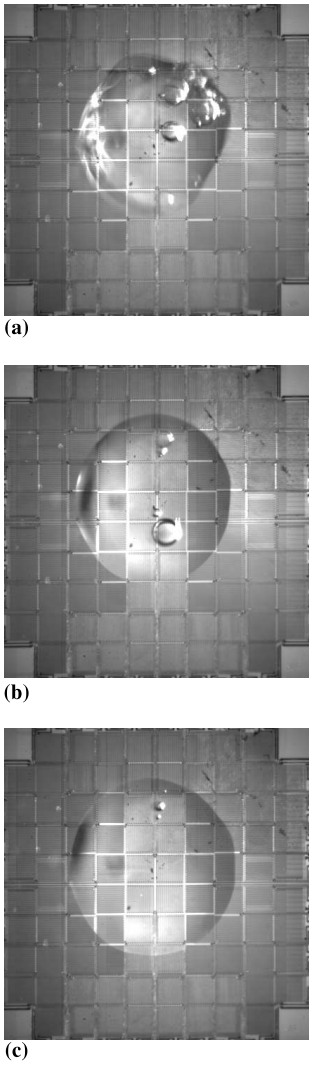

Fig. 6. Droplets at (a) 85°C, (b) 75°C and (c) 65°C at 100 ms.

Shown in Table 3 is the ratio of d_0 to d_{eq}. This ratio is very close to unity, suggesting that the measurements are accurate. d_{eq} is seen to be slightly larger than d_0, which is impossible, but the discrepancy could easily be due to improper fluid property values and/or errors in measuring the droplet diameter. In fact, the uncertainty in droplet diameter alone accounts for much of the discrepancy.

5.4. Time resolved heat rate

The time-resolved heat transfer variation from the array at the three superheats is shown in Fig. 8. The ordinate was obtained using the following equation:

$$q(t) = \sum_{i=1}^{N} q_i''(t) A_i, \tag{13}$$

where $q_i''(t)$ is the wall heat flux at time t for heater i corrected for substrate conduction. It is seen that the droplet evaporation time decreases with increasing wall temperature, as would be expected. The heat rate $q(t)$ trace for a wall temperature of 85°C contains a high-frequency component from droplet impact to about 0.42 s. Correlation with the high-speed video indicated that this activity was due to nucleate boiling within the splat. Very few bubbles were observed after 0.42 s at this superheat. After 0.42 s, the heat transfer suddenly decreased, indicating the end of boiling. The minimum film thickness to support nucleate boiling was theoretically suggested by Chen et al. (1977):

$$\delta_{\min} = \frac{8\sigma T_{sat}}{\rho_v h_{fg}(T_w - T_{sat})}. \tag{14}$$

Using the properties of PF-5060 with a wall temperature of 85°C, Eq. (14) gives a value of 1 μm for the minimum thickness to support boiling. Estimating the remaining drop volume at this time using the amount of energy transferred to the droplet reveals that approximately 10% of the original droplet volume remained, giving an average splat thickness of 85 μm. The source of this discrepancy is currently not understood. The droplet behavior at this superheat could be classified as belonging to the intermediate superheat regime. The heat flux traces for wall temperatures of 75°C and 65°C do not contain any high-frequency activity, indicating little boiling within the splat – this behavior is consistent with droplet evaporation in the low superheat regime.

The time-resolved heat transfer distributions along with β shortly after impact ($0 < t < 100$ ms) is shown in Fig. 9. The data is seen to be remarkably repeatable from drop to drop at all temperatures. For $0 < t < 20$ ms, the tested data show oscillations in the heat flux level whose peaks and valleys correspond with the oscillations in the spread ratio, β.

5.5. Droplet thermal resistance

The droplet heat transfer is determined by the thermal resistance within the liquid ($R_l = \delta/kA_D$) and the resistance associated with vapor removal from the top of the droplet ($R_v = 1/h_v A_D$) as indicated on Fig. 10. The total heat transfer coefficient (h) is related to the thermal resistances by

$$R_{th} = R_l + R_v = \frac{1}{hA_D}. \tag{15}$$

As a droplet evaporates, R_l decreases since the thickness of the splat decreases. Just before the final liquid evaporates, the total thermal resistance is dominated by R_v.

The variation in heat transfer coefficient with time can be computed using the data from Eq. (1). In terms of the droplet variables, h is given by

$$h(t) = \frac{4}{(T_w - T_a)} \frac{q(t)}{\pi d_0^2 \beta(t)^2}. \tag{16}$$

Plots of the variation in $h(t)$ is shown on Fig. 11. It is seen that h is relatively constant for $0.2 < t^* < 1.0$ for all three wall temperatures. The significance of a constant h over this period is that it indicates that thermal resistance within the liquid is negligible compared to the thermal resistance associated with vapor removal. If the thermal resistance in the liquid was important, then a rise in h should have been observed as the droplet evaporates since R_l decreases as the droplet thins. The results show that in order to increase the heat transfer coefficient, one must increase the rate at which vapor is removed from the top of the drop, consistent with the findings of Qiao and Chandra (1997), Di Marzo and Evans (1989), and De Marzo et al. (1993).

For $0 < t^* < 0.2$, however, a transient spike in the value of h is observed (see Fig. 12). It is of interest to note that the transients all appear to collapse onto the same curve when plotted against dimensional time, indicating that the early evolution of h depends linearly on the temperature difference, and does not depend on the total evaporation time of the

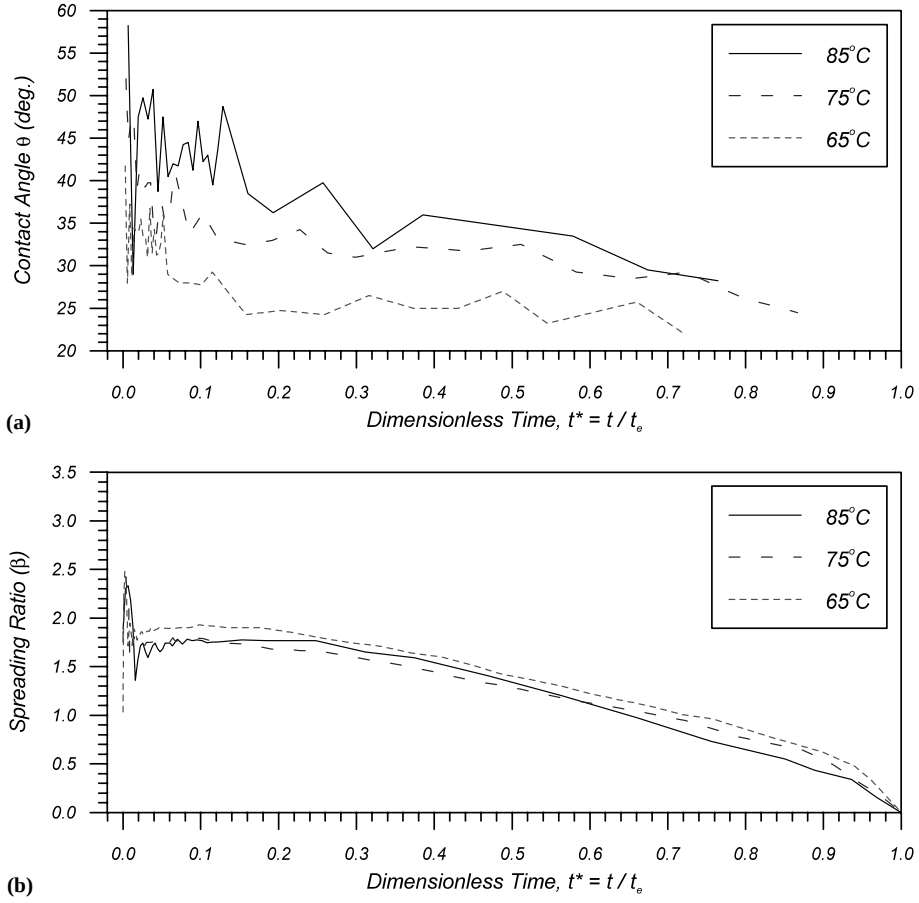

Fig. 7. Variations in time-resolved liquid–solid contact angle and spreading ratio after impact, normalized on droplet evaporation time: (a) liquid–solid contact angle, θ; (b) spreading ratio, β.

Table 3
Comparison between experimental results and energy balances

T_w (°C)	$t_e(s)$	Q_{meas} (J)	d (mm)	d_{eq} (mm)	d/d_{eq} (%)
85	0.63	0.069	0.82	0.87	95
75	1.13	0.062	0.83	0.84	99
65	1.55	0.061	0.82	0.83	98

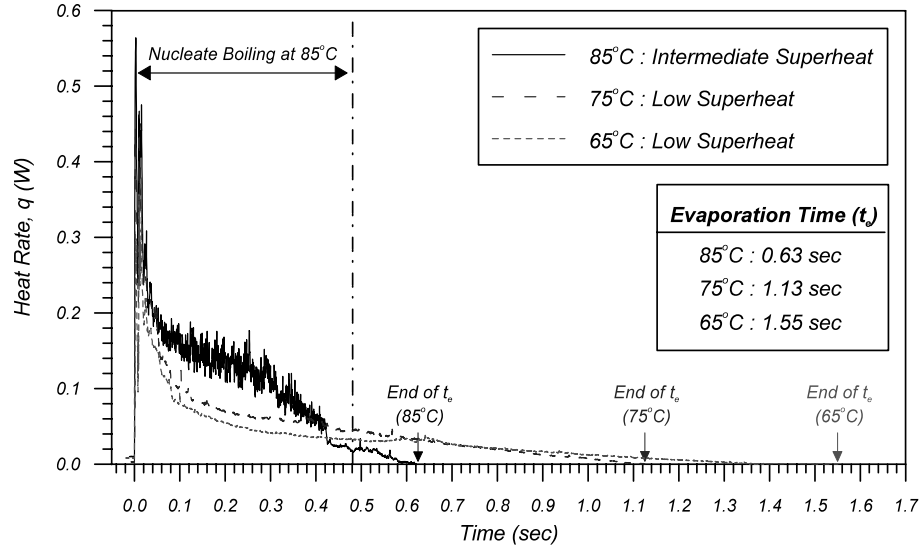

Fig. 8. Time-resolved distributions in rate of heat with $T_w = 85°C$, 75°C, and 65°C.

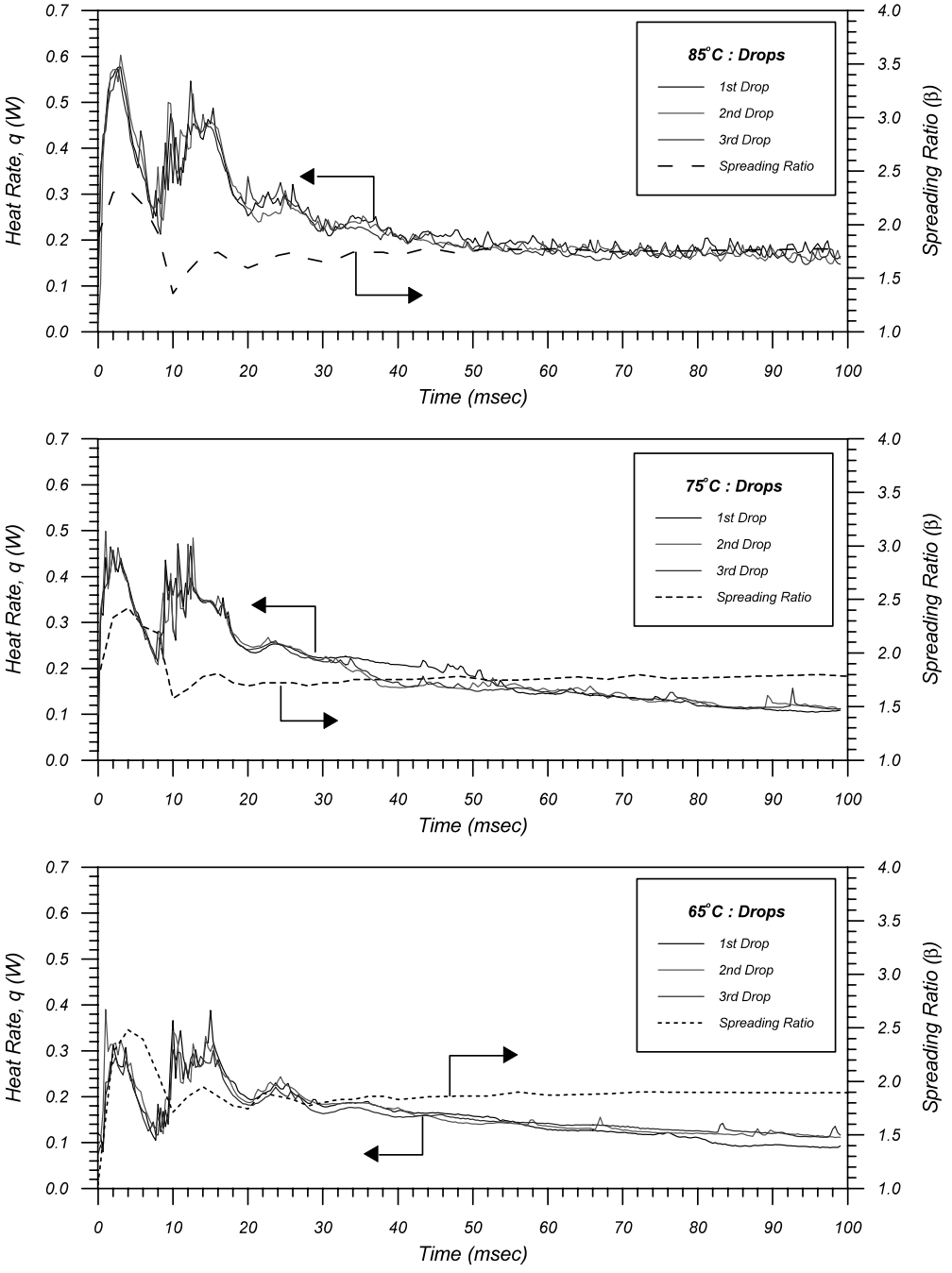

Fig. 9. Time-resolved heat rate distributions after impact for 0.1 s (T_w = 85°C, 75°C, and 65°C).

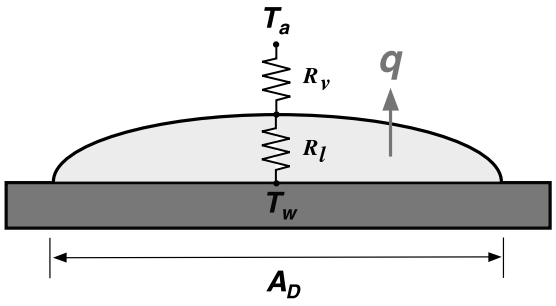

Fig. 10. Schematic of the droplet resistance.

droplet. Several possible mechanisms may be responsible for this behavior. First, this behavior might be caused by transient conduction heating of the droplet from its original ambient temperature to its saturation temperature. This can be checked by approximating the droplet as a semi-infinite solid that is suddenly subject to a step change in wall temperature, and calculating the transient heat flux that would occur across its boundary. If one assumes the mass transfer effects to be relatively weak at the ambient temperatures, then the solution should remain valid until the heat wave just begins to reach the outer surface of the drop and starts to increase the temperature of the gas/liquid interface above the initial value T_0. Using the properties of PF-5060, the transient heat transfer coefficient

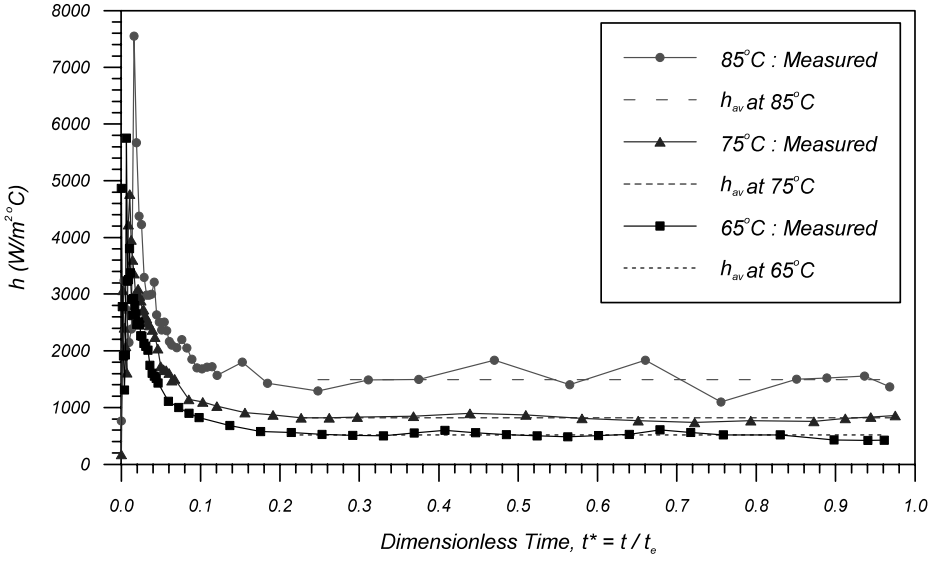

Fig. 11. Time-resolved heat transfer coefficient (h) during evaporation time, t_e, and average heat transfer coefficient (h_{av}) at $T_w = 85°C$, 75°C, and 65°C.

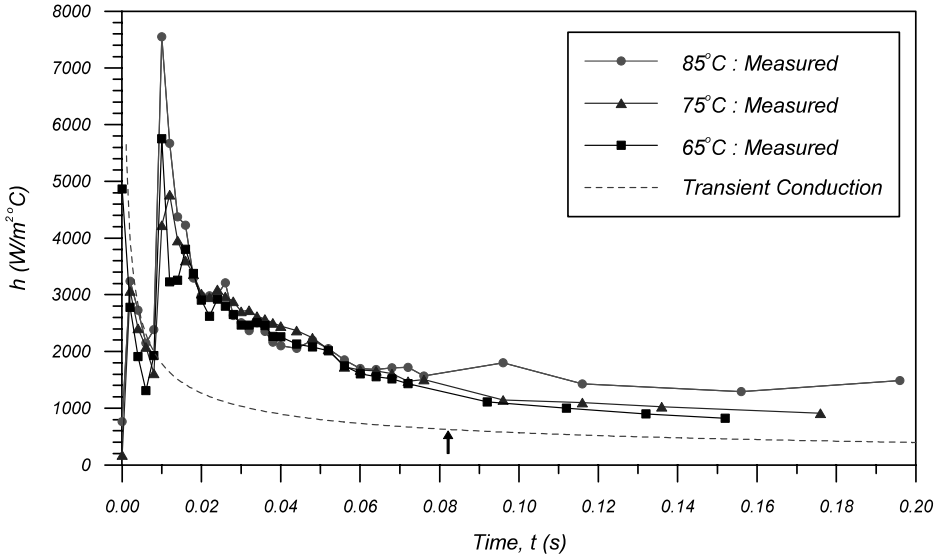

Fig. 12. Detail view of heat transfer coefficient.

for such conditions are plotted in Fig. 12. Assuming the droplet to be a disk of uniform thickness consistent with the initial droplet volume and contact area, the time at which the heat wave first reaches the upper surface of the hypothetical splat is indicated by the arrow (assumed to occur when the surface temperature has increased by 2% of the initial temperature difference). From this result, one sees a qualitative agreement during the first 6 to 8 ms when the droplet initially contacts the surface. After 8 ms, however, the heat transfer coefficient increases sharply, and resumes a more gradual decay with a few minor oscillations before reaching its steady-state value at $t = 150$ ms. The second sharp increase in h corresponds to a time during which the heat flux is rapidly rising, but β is still rapidly decreasing (see Fig. 9, between 8 and 12 ms). Although the transient conduction profile tracks the general shape of the second decay event, the actual decay event is obviously complicated by additional effects such as the oscillatory motion within the drop.

A second possible cause for the variation in h may reflect a change in R_v due to a change in the concentration gradient at the liquid/vapor interface. Vapor removal from the top of the drop occurs primarily by diffusion in this experiment since there was little air movement over the drop. When the drop first impacts the surface, rapid vapor removal occurs since the concentration gradient is steep. As liquid evaporates, however, the concentration boundary layer thickens, decreasing the concentration gradient and therefore the vapor removal rate.

Third, bubbles within the drop that occur due to degassing of the fluid might have the effect of increasing the surface area at the top of the drop, allowing vapor to leave the surface more readily, thus decreasing R_{th} and increasing h. As degassing of

the fluid occurs, the bubble size decreases along with the surface area, resulting in a decrease in h.

Future models need to include such effects to accurately capture the early history of the evaporation transient. Qiao and Chandra (1997), Di Marzo and Evans (1989), and De Marzo et al. (1993) did not observe these strong transients in h during the first stage of evaporation, probably because the drops in their studies took much longer to evaporate than those in this study.

Table 4
Comparison between calculated and measured average heat transfer coefficient

T_w (°C)	h_{av} (W/m^2 °C)	h_{cal} (W/m^2 °C)	h_{av}/h_{cal} (%)
85	1488	1498	99
75	814	822	99
65	515	523	98

5.6. Comparison to two stage model

The non-uniform heat transfer coefficient observed during the first stage of the evaporation process indicates that the first stage evaporation model cannot be applied to these droplets. As shown in Fig. 11, the assumption in constant heat transfer coefficient h can be applied only at the second stage, proposed by Di Marzo and Evans (1989), De Marzo et al. (1993), and Qiao and Chandra (1997). During the second stage, the calculated heat transfer coefficient h_{cal} can be estimated from Eq. (4) assuming $t_e = t_{e2}$ and V_0 equal to the volume of the droplet at the beginning of the second stage (computed using Eq. (3) with $\theta = \theta_r$ and D equal to the splat diameter at the beginning of the second stage). The average

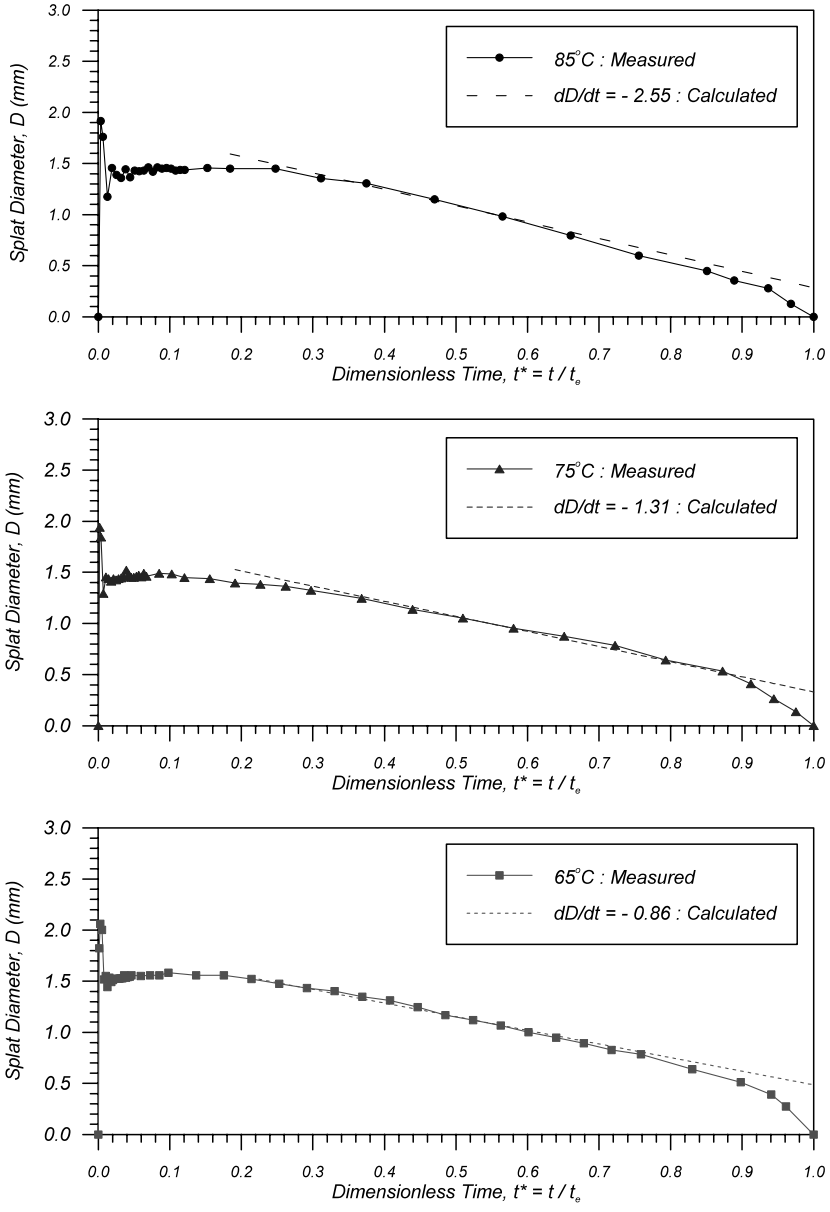

Fig. 13. Comparison between model and measured splat diameter in second stage.

Table 5
Comparison between estimated and measured second evaporation time

T_w (°C)	$t_{e2,meas}$ (s)	$t_{e2,cal}$ (s)	$t_{e2,meas}/t_{e2,cal}$ (%)
85	0.47	0.58	81
75	0.85	1.09	78
65	1.16	1.62	72

drop area A_{av} is equal to the average splat area during the second stage ($A_{av,2}$):

$$A_{av,2} = \frac{1}{t_{e2}} \int_{t_{e1}}^{t_e} \frac{\pi}{4} d_0^2 \beta^2(t)\, dt. \quad (17)$$

Comparison of the calculated value h_{cal} is made with the measured value h_{av} on Table 4. Very good agreement is observed, indicating that the second stage model is quite accurate.

For the second stage of evaporation, the rate of change in splat diameter during the second stage can be computed using Eq. (9). Comparison to the data can be performed by drawing a line with the slope given by Eq. (9) through a data point in the middle of the second stage as seen on Fig. 13. The value of θ_r and h_{av} used in the computation was the average between $0.2 < t^* < 1.0$ in Figs. 7 and 11, respectively. The good agreement between the computed line and the data indicates that the second stage model predicts quite well the variation in splat diameter with time during the droplet evaporation process.

The second stage evaporation time t_{e2} can be predicted using Eq. (10) for known values of D_0, h_{av}, and θ_r. The estimated values of t_{e2} are compared with the measured values on Table 5. It is seen that the measured values are somewhat smaller than predicted. The discrepancy is probably due to the rapid decrease in the splat diameter towards the end of the evaporation time as seen in Fig. 13. The reason for this is currently not known.

6. Conclusions

An experimental technique using an array of microscale heaters and high-speed imaging has been used to examine the time- and space-resolved heat flux and dynamics of the droplet vaporization process on an isothermal wall. The experiments were performed with a working fluid of PF-5060 in ambient air, with a fixed impact diameter (0.82 mm) and velocity (0.3 m/s), but at three different superheats ($T_w - T_{sat} = 9$°C, 19°C and 29°C). When the heat flux data is expressed in terms of an effective heat transfer coefficient, h, the results show that the droplet vaporization process can be divided into two distinct parts: the first part corresponds to a transient fluctuation of h, while the second is characterized by a constant value of h. The initial transient is likely to be caused by a combination of the initial heat conduction into the liquid, the oscillatory motion of the droplet, and the establishment of a vapor concentration boundary layer at the liquid–vapor interface. The present work was not able to discern the exact contribution from each of these components, which is the focus of study for continuing work. The second part of the vaporization process, corresponding to a constant h, is consistent with a perspective in which the heat transfer rate is limited by the external diffusion/convection resistance of the vapor away from the droplet. Comparisons made to the constant contact angle (moving contact line) models of De Marzo et al. (1993) and Qiao and Chandra (1997), which require a constant effective h, give very good agreement for the rate of change of the splat diameter during this regime, until the final 10% of the evaporation time. Thus for droplets with these specific impact conditions, the existing models for low superheat vaporization are adequate to predict approximately 65% of the droplet's lifetime. Continued work needs to be focused on the prediction of the transient h regime, particularly if advances are to be made in spray cooling applications where the droplets are typically much smaller. Under these conditions, the droplet evaporation process may be short enough such that it is wholly dominated by the transient process.

Acknowledgements

This work was jointly supported by the Air Force Research Laboratory (AFRL), Wright Patterson Air Force Base, Dayton, OH under the grant F33615-98-1-2791 and the Laboratory for Physical Sciences (LPS), College Park, MD. The authors wish to express their gratitude to Dr. R. Ponnappan (AFRL), Dr. J. Leland (AFRL), and Dr. P. Boudreaux (LPS) for their encouragement and support throughout this study.

References

3M Corporation, 1995. 3M Specialty Fluids Newsletter, vol. 1 (1).
Bae, S., Kim, M.H., Kim, J., 1999. Improved technique to measure time- and space-resolved heat transfer under single bubbles during saturated pool boiling of FC-72. Exp. Heat Transfer 12, 265–278.
Bolle, L., Moureau, J.C., 1982. Spray Cooling of Hot Surfaces, Multiphase Science and Technology, vol. 1. Hemisphere, Washington, DC, pp. 1–97.
Bonacina, C., Giudice, S., Comini, G., 1979. Dropwise evaporation. J. Heat Transfer 101, 441–446.
Chen, J.C., Sundaram, R.K., Ozkaynak, F.T., 1977. A phenomenological correlation for post-CHF heat transfer. Technical Report for USNRC, Contract No. AT(49-24)-0180, Lehigh University, Bethlehem, PA.
Choi, K.J., Yao, S.C., 1987. Mechanism of film boiling heat transfer of normally impacting spray. Int. J. Heat Mass Transfer 30, 311–318.
Di Marzo, M., Evans, D.D., 1989. Evaporation of a water droplet deposited on a hot high thermal conductivity surface. J. Heat Transfer 111, 210–221.
De Marzo, M., Tartarini, P., Liao, Y., Evans, D., Baum, H., 1993. Evaporative cooling due to a gently deposited droplet. Int. J. Heat Mass Transfer 36, 4133–4139.
Kline, S.J., McClintock, F.A., 1953. Describing uncertainties in single-sample experiments. Mech. Eng. 75, 3–8.
Liu, L., Yao, S.C., 1982. Heat transfer analysis of droplet flow impinging on a hot surface. In: Proceedings of the Seventh International Heat Transfer Conference, vol. 4. Munich, Germany, pp. 161–166.
McGinnis, F.K., Holman, J.P., 1969. Individual droplet heat transfer rates for splattering on hot surfaces. Int. J. Heat Mass Transfer 12, 95–108.
Qiao, Y.M., Chandra, S., 1997. Experiment on adding a surfactant to water drops boiling on a hot surface. Proc. Roy. Soc. London A 453, 673–689.
Rule, T.D., Kim, J., 1999. Heat transfer behavior on small horizontal heaters during pool boiling of FC-72. J. Heat Transfer 121, 386–393.
Rule, T.D., Kim, J., Kalkur, T.S., 1998. Design, construction, and qualification of a microscale heater array for use in boiling heat transfer, NASA/CR-1998-207407.

Rule, T.D., Kim, J., Quine, R.W., Kalkur, T.S., Chung, J.N., 1999. Measurements of spatially and temporally resolved heat transfer coefficients in subcooled pool boiling. In: Convective Flow and Pool Boiling. Taylor & Francis, London.

Sadhal, S.S., Ayyaswamy, P.S., Chung, J.N., 1997. Transport Phenomena with Drops and Bubbles. Springer, New York.

Sadhal, S.S., Plesset, M.S., 1979. Effect of solid properties and contact angle in dropwise condensation and evaporation. J. Heat Transfer 101, 48–54.

Toda, S., 1972. A study of mist cooling (second report: investigation of mist cooling). Heat Transfer-Japanese Res. 1, 39–50.

Toda, S., 1974. A study of mist cooling (first report: theory of mist cooling and its fundamental experiments). Heat Transfer-Japanese Res. 3, 1–44.

Wachters, L.H.J., Bonne, H., Nouhuis, H.J., 1966. The heat transfer from a hot horizontal plate to sessile water drops in the spheroidal state. Chem. Eng. Sci. 21, 923–936.

Wachters, L.H.J., Westerling, N.A.J., 1966. The heat transfer from a hot wall to impinging water drops in the spheroidal state. Chem. Eng. Sci. 21, 1047–1056.